Molecular Therapy
Nucleic Acids
Original Article

Cancer-derived exosome miRNAs induce skeletal muscle wasting by Bcl-2-mediated apoptosis in colon cancer cachexia

Chunxiao Miao,[1,2,5] Wanli Zhang,[1,5] Lixing Feng,[1] Xiaofan Gu,[1] Qiang Shen,[1,3] Shanshan Lu,[1] Meng Fan,[1] Yiwei Li,[1] Xianling Guo,[4] Yushui Ma,[1] Xuan Liu,[3] Hui Wang,[4] and Xiongwen Zhang[1]

[1]Shanghai Engineering Research Center of Molecular Therapeutics and New Drug Development, School of Chemistry and Molecular Engineering, East China Normal University, Shanghai, China; [2]State Key Laboratory of Oncogenes and Related Genes, Shanghai Cancer Institute, Renji Hospital, Shanghai Jiaotong University School of Medicine, Shanghai, China; [3]Institute of Interdisciplinary Integrative Biomedical Research, Shanghai University of Traditional Chinese Medicine, Shanghai, China; [4]Department of Oncology, The Tenth People's Hospital, Tongji University, Shanghai, China

Cancer cachexia is a kind of whole-body metabolic disorder syndrome accompanied by severe wasting of muscle tissue in which cancer exosomes may be involved. Analysis of clinical samples showed that the serum exosome concentrations were correlated with the development of cancer cachexia. Exosomes secreted by C26 cells could decrease the diameter of C2C12 myotubes *in vitro* and decrease mouse muscle strength and tibialis anterior (TA) muscle weight *in vivo*. GW4869, an inhibitor of exosome excretion, ameliorated muscle wasting in C26 tumor-bearing mice. MicroRNA (miRNA) sequencing (miRNA-seq) analysis suggested that miR-195a-5p and miR-125b-1-3p were richer in C26 exosomes than in exosomes secreted from MC38 cells (non-cachexic). Both miR-195a-5p and miR-125b-1-3p mimics could induce atrophy of C2C12 myoblasts. Downregulation of Bcl-2 and activation of the apoptotic signaling pathway were observed in C2C12 myoblasts transfected with miR-195a-5p and miR-125b-1-3p mimics, in the gastrocnemius muscle of C26 tumor-bearing mice and in the TA muscle injected with C26 exosomes. Results of dual-luciferase assay confirmed the targeting of miR-195a-5p/miR-125b-1-3p to Bcl-2. Overexpression of Bcl-2 successfully reversed atrophy of C2C12 myoblasts induced by the two miRNA mimics. These results suggested that cancer exosome enriched miRNAs might induce muscle atrophy by targeting Bcl-2-mediated apoptosis.

INTRODUCTION

Cachexia is a severe wasting syndrome accompanied by serious loss of body weight during a lot of chronic diseases such as cancer, AIDS, and tuberculosis.[1] Cancer cachexia affects ~50%–80% of advanced cancer patients and is mainly characterized by fatigue, loss of muscle and fat, and systemic inflammation.[2,3] Skeletal muscle consumption is the most obvious feature of cancer cachexia. Cancer cachexia not only influences patients' quality of life but also weakens the efficacy of chemotherapy and radiotherapy on tumor, therefore decreasing patients' survival time seriously.

Skeletal muscle loss is one of the most obvious and main symptoms of cachexia, which is mainly caused by the enhancement of protein degradation. In addition to the ubiquitin-proteasome pathway and the autophagy-lysosome pathway, the apoptosis pathway is also an important pathway to promote protein degradation during muscle atrophy. Apoptosis is a process that has been found to be important for controlling muscle mass loss, which could be activated during cachexia. Sílvia Busquets et al. found that apoptosis occurs in human skeletal muscle undergoing cancer cachexia.[4] Apoptosis is present in skeletal muscle of cachectic gastro-intestinal cancer patients.[5] Apoptosis markers were observed in severely cachectic muscle of Apc (Min/+) mice.[6]

Multiple factors secreted by body and cancer cells, including inflammation cytokines, contribute to the occurrence of cancer cachexia.[7–9] Recent studies suggested that cancer exosomes might also be involved in the development of cancer cachexia.[10–14] Cancer exosomes are nanometer-sized vesicle-like bodies secreted by cancer cells into the extracellular environment, and they participate in the transfer of materials and information between the tumor and tumor microenvironment. Exosomal proteins, lipids, and nucleic acids (DNA, mRNA, microRNA [miRNA], long non-coding RNA [lncRNA], etc.) might participate in the biological process of cancer cachexia in many ways.[10,15,16] Previous studies suggest that exosomes secreted by cancer cells and miRNAs in exosomes might participate in the

Received 25 November 2020; accepted 20 April 2021;
https://doi.org/10.1016/j.omtn.2021.04.015.

[5]These authors contributed equally

Correspondence: Xuan Liu, Institute of Interdisciplinary Integrative Biomedical Research, Shanghai University of Traditional Chinese Medicine, Shanghai, China.
E-mail: xuanliu@shutcm.edu.cn
Correspondence: Hui Wang, Department of Oncology, The Tenth People's Hospital, Tongji University, Shanghai, China.
E-mail: wanghui_ys@sina.com
Correspondence: Xiongwen Zhang, Shanghai Engineering Research Center of Molecular Therapeutics and New Drug Development, School of Chemistry and Molecular Engineering, East China Normal University, Shanghai, China.
E-mail: xwzhang@sat.ecnu.edu.cn

Table 1. A colon cancer cachexia stating score to classify cachexia stages

Measurements	Values	Point
Weight loss in 6 months	weight stable or weight loss ≤ 5%	0
	weight loss ≥ 5% and < 10%	1
	weight loss ≥ 10% and < 15%	2
	weight loss ≥ 15%	3
ECOG PS	0	0
	1–2	1
	3–4	2
Abnormal biochemistry	all normal	0
Alb < 35 g/L	one of three abnormal	1
② Electrolyte imbalance	two of three abnormal	2
③ Liver and kidney dysfunction	all abnormal	3

ECOG PS, Eastern Cooperative Oncology Group performance status; Alb, albumin.

regulation of skeletal muscle wasting in the development of cancer cachexia.[9–11,14,17] For example, miR-21 and miR-26a in exosomes had been shown to induce muscle wasting. MV Cargo miR-21 promotes apoptosis through JNK activation to promote muscle wasting.[18] Exosomes containing miR-26a prevented muscle atrophy by inhibiting the transcription factor forkhead box O1.[19] Exo/miR-26a decreased the upregulation of FBXO32/atrogin-1 and TRIM63/MuRF1 to limit muscle wasting in chronic kidney disease.[20]

These reports suggested the important roles of cancer exosomes and their active miRNAs in development of cancer cachexia, but the detailed mechanisms have not been clarified. It is possible that specific active components in cancer exosomes might be varied in different types of cancer, which could regulate different targets and signal pathways during cancer cachexia.

In the present study, we concentrated on clarifying the roles and mechanisms of cancer exosomes and their active miRNAs in the development of colon cancer cachexia. The serum exosome concentrations of healthy persons and colon cancer patients with or without cachexia were analyzed to check the possible correlation between exosomes and cachexia. Then, a further study was conducted using *in vitro* and *in vivo* cancer cachexia models induced by C26 colon cancer cells, which have been popularly used in cancer cachexia studies.[21] At the same time, the MC38 colon cancer cell line, which was reported to be a kind of non-cachectic cancer cell line, was used as a negative control cell line in comparison with the C26 cell line.[22,23] The capabilities of C26 cells and MC38 cells to induce muscle wasting *in vivo* and *in vitro* were checked, and the functions of C26 exosomes and MC38 exosomes during cancer cachexia were also compared *in vivo* and *in vitro*. Furthermore, to search for possible active miRNAs in C26 exosomes, miRNA profiles of C26 exosomes and MC38 exosomes were analyzed using miRNA sequencing (miRNA-seq) technology. The activities of two miRNAs (miR-195a-5p and miR-125b-1-3p) enriched in C26 exosomes in inducing muscular wasting were further observed. The possible target genes of the two active miRNAs and downstream signaling pathway were then investigated in C2C12 cells treated with miR-195a-5p mimic or miR-125b-1-3p mimic. The experimental procedures and findings are reported as follows.

RESULTS

Cancer exosomes participated in cancer cachexia

In order to prove the correlation between exosomes and the cancer cachexia process, we collected serum from clinical patients with or without colon tumor. To simplify the criteria of colon cancer cachexia stages, we defined a colon cancer cachexia staging score (CSS) for clinical use.[24] The CSS consists of three components (Table 1): weight loss in 6 months (score range: 0–3), ECOG (Eastern Cooperative Oncology Group) performance status (score range: 0–2), and abnormal biochemistry (score range: 0–3). Patients with colon tumor were classified into two stages of cachexia: non-cachexia (score range: 0–5) and cachexia (score range: 6–8). All clinical serum samples included healthy subjects (19 cases) and non-cachexia (13 cases) and cachexia (8 cases) patients with colon cancer (Table 2). The exosomes isolated from serum of all clinical serum samples were analyzed by electron microscopy (Figure 1A). Utilizing a Zeta nanoparticle tracking analyzer, we observed that the diameter of exosomes from patients was ~25–75 nm (Figure 1B). Exosomes were detected with an acetylcholinesterase (AchE) assay kit (Figure 1C). Results showed that the contents of exosomes from patient serum increased accompanied by the development of cancer cachexia, which suggested that exosomes were involved in the progression of cancer cachexia.

C26 but not MC38 colon cancer cells induced skeletal muscle atrophy *in vitro* and *in vivo*

We compared differences of the ability to induce cachexia between C26 and MC38 *in vivo* and *in vitro*. C2C12 myotubes were incubated with culture medium of MC38 and C26 cancer cells respectively for 48 h. As shown in Figures 2A (representative result) and 2B (statistical analysis result), incubation of C26 medium but not MC38 medium induced significant decrease in the diameter of C2C12 myotubes. The diameters of C2C12 myotubes in the C26 medium-treated group and the MC38 medium-treated group were about 69.7% and 90% of that of the control group, respectively. The results suggested that C26 medium but not MC38 medium could induce C2C12 myotube atrophy.

Likewise, results of an *in vivo* study showed that inoculation of C26 cells induced significant decrease in tumor-free weight of mice, and the tumor-free weight decreased ~10% at the end of the experiment, day 16 after the inoculation (Figure 2C). On the contrary, inoculation of MC38 cells did not induce significant decrease in tumor-free weight of mice, and the tumor-free weight decreased <1% at the end of the experiment, day 24 after the inoculation (Figure 2D). Although the growth of MC38 tumor was lower than that of C26 tumor, the volume of MC38 tumor at the end of the experiment was similar to that of C26 tumor (Figures S1A and S1B). These results suggested that the difference between the weight loss in C26 tumor-bearing mice and that in MC38 tumor-bearing mice was not related

Table 2. Demographic and selected clinical data with colon cancer for study

Group	Non-cachexia (n = 13)	Cachexia (n = 8)
Male:female	12:1	5:3
Age (years)	64 (42–85)	61 (50–75)
Weight loss in 6 months	11/13 (0–10%)	0/8 (0–10%)
	1/13 (10–15%)	2/8 (10–15%)
	1/13 (15–25%)	6/8 (15–25%)
ECOG PS	7/13 (score 0–2)	0/8 (score 0–2)
	6/13 (score 3)	8/8 (score 3)
Abnormal biochemistry		
Alb < 35 g/L	8/13	8/8
② Electrolyte imbalance	3/13	5/8
③ Liver and kidney dysfunction	3/13	6/8
Score range		
0–3	8/13	0/8
4–5	5/13	0/8
6–7	0/13	6/8
8	0/13	2/8

Patients with colon tumor were classified into two stages of cachexia: non-cachexia (score range: 0–5) and cachexia (score range: 6–8).

to tumor growth but might have resulted from the difference in the capability of the two kinds of cells to induce cachexia. Gastrocnemius (GA) weight, body temperature, and grip strength of C26 tumor-bearing mice were significantly lower than those in the healthy group, whereas there was no difference between MC38 tumor-bearing mice and the healthy group (Figures 2E and 2F; Figures S1C and S1D).

These results demonstrated that C26 but not MC38 tumor cells could induce skeletal muscle atrophy *in vitro* and *in vivo*. Therefore, in the following experiments, MC38 cells were used as a negative control model of colon cancer cachexia *in vitro* and *in vivo*.

C26 cancer-derived exosomes induced skeletal muscle atrophy *in vitro*

We analyzed concentrations of exosomes in C26 tumor-bearing mice and MC38 tumor-bearing mice. As shown in Figure 3A, the serum exosome concentration of C26 tumor-bearing mice is significantly higher than that of the healthy group. On the contrary, there was no difference between MC38 tumor-bearing mice and the healthy group (Figure 3A). These results suggested the possible involvement of C26 tumor exosomes in inducing cachexia in C26 tumor-bearing mice.

In order to analyze the relationship between cancer exosomes and cachexia, we purified C26 exosomes and MC38 exosomes from culture medium of C26 and MC38 cells, respectively, which were examined by immunoblotting using the antibody against CD9 and CD63, electron microscopy, and the Zeta nanoparticle tracking analyzer (Figures 3B–3D). As shown in Figures 3B and 3C, both C26 exosomes and MC38 exosomes exhibited saucer-like bilayer membrane structure, and their diameters were ~100 nm. There was no significant difference between the diameters of C26 exosomes and MC38 exosomes, though MC38 exosomes might be a little bigger than C26 exosomes. Results of analysis of exosome concentration in C26 and MC38 tumor medium with the AchE assay kit showed that exosome concentration in the C26 tumor medium is significantly higher than that in MC38 tumor medium (Figure 3E). The results were in accordance with the results of exosome concentration analysis in C26 tumor-bearing mouse serum and MC38 tumor-bearing mouse serum.

In order to check the direct effects of exosomes on skeletal muscle atrophy, C2C12 myotubes were treated with C26 exosomes or MC38 exosomes for 48 h. As shown in Figure S2A, exosomes were successfully absorbed by C2C12 myotubes. While only C26 exosomes were able to induce C2C12 myotube atrophy, the diameter of myotubes and the protein expression of MHC in C26 exosome-treated C2C12 myotubes were significantly decreased compared with MC38 exosome-treated C2C12 myotubes (Figures 3F–3H). The effects of C26 exosomes on C2C12 myotubes were dose dependent, since the diameter of C2C12 myotubes gradually decreased along with the increase of C26 exosome concentrations (Figures S2B and S2C). Similarly, HT-29 exosomes were also able to induce C2C12 myotube atrophy instead of SW480 (non-cachexic) exosomes (Figure S3). GW4869, an inhibitor of exosome excretion,[25,26] was used in the present study to further confirm the effects of C26 exosomes on muscle atrophy. As shown in Figure 3I, the excretion of C26 exosomes could be blocked by GW4869 treatment, and the exosome concentration in C26 tumor medium decreased with the increase of GW4869 dose. Accordingly, the pro-atrophy ability of C26 tumor medium was inhibited by GW4869; thus the diameter of myotubes and the MHC protein expression of the GW4869-treated C26 group were higher than the control C26 group (Figures 3J–3L). These results suggested that C26 exosomes were involved in the effects of C26 medium in inducing skeletal muscle atrophy *in vitro*.

C26 exosomes induced skeletal muscle atrophy *in vivo*

Inhibition of C26 exosome excretion could alleviate C2C12 myotube atrophy *in vitro* (Figures 4A and 4B). *In vivo*, we found that GW4869 treatment (intra-tumor injection) did not affect C26 tumor growth and the tumor-free weight of mice (Figures 4A and 4B) but effectively alleviated the loss in tibialis anterior (TA) muscle weight and the weakening of TA grip strength in C26 tumor-bearing mice (Figures 4C–4E). These results suggested that C26 exosomes were involved in the effects of C26 tumor in inducing skeletal muscle atrophy *in vivo*.

In order to observe the effects of C26 exosomes on skeletal muscle atrophy *in vivo* directly, purified C26 exosomes (50 μL) were injected directly into the TA muscle of left hindlimbs of mice once every other day for 22 days. The grip strength of left hindlimbs was measured at day 10 and day 22. High doses of C26 exosome (2×) intramuscular injection could significantly decrease the muscle strength and the weight of the TA muscle (Figures 4F and 4G). These results suggested

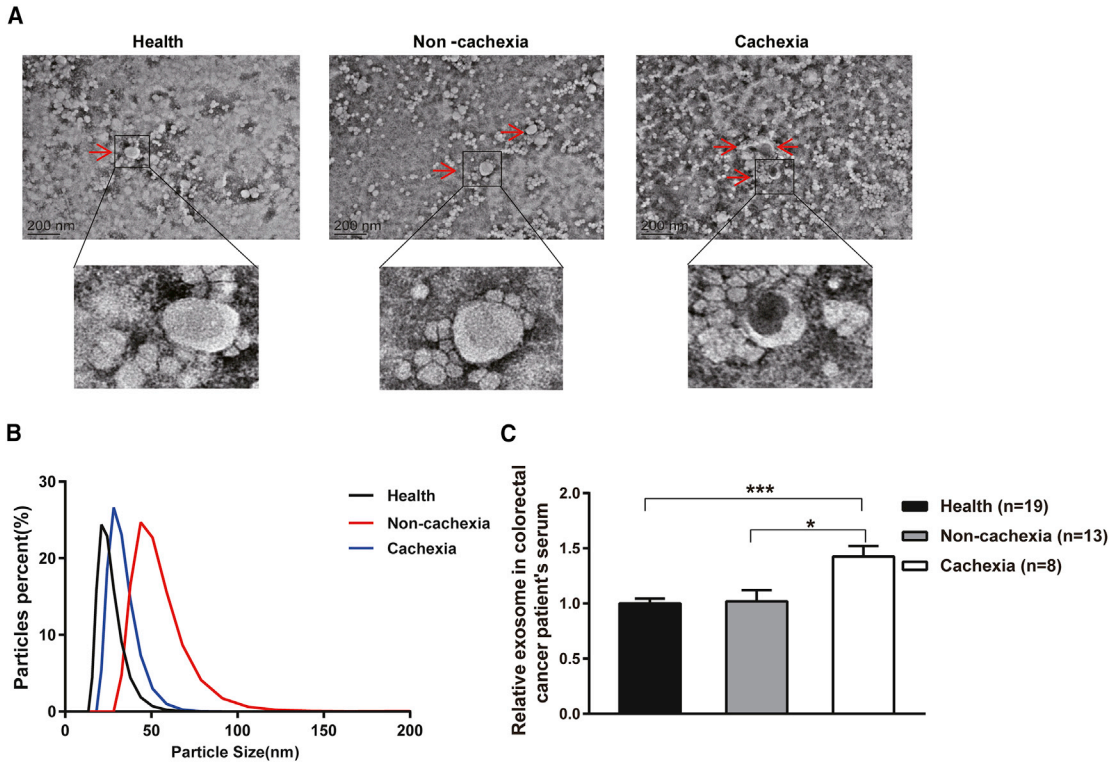

Figure 1. Analysis of serum exosomes from healthy persons and non-cachexia and cachexia patients with colon cancer

(A) Electron microscopy images of serum exosomes from healthy persons and non-cachexia and cachexia patients with colon cancer (scale bars, 200 nm). (B) Exosome particle size analysis of exosomes from serum of healthy persons and non-cachexia and cachexia patients with colon cancer. (C) The content of exosomes in equal amounts of clinical serum samples (healthy, non-cachexia, and cachexia) were detected with the AchE Assay Kit. Data presented are the mean ± SEM of three independent experiments. *$p < 0.05$, ***$p < 0.001$.

that C26 exosomes could directly induce skeletal muscle atrophy *in vivo*.

C26 exosomal miRNAs regulated skeletal muscle atrophy

To identify the active molecules in C26 exosomes that induce skeletal muscle atrophy *in vitro* and *in vivo*, we took advantage of miRNA-seq to compare the miRNA profiles of C26 exosomes and MC38 exosomes (GEO: GSE173202). C2C12 myotubes were treated with many kinds of miRNA (high fold change) mimics, and we found that miR-195a-5p and miR-125b-1-3p had the strongest ability to induce atrophy of C2C12 myotubes (Figure 5A; Figure S4). Results of miRNA-seq suggested that the levels of miR-195a-5p and miR-125b-1-3p in C26 exosomes were higher than those in MC38 exosomes (Figure 5A), and results of qPCR analysis also confirmed the high levels of the two miRNAs in C26 exosomes (Figure 5B), which were higher in HT-29 exosomes than in SW480 exosomes (Figure S3D). In line with this, the levels of miR-195a-5p and miR-125b-1-3p were significantly higher in C26 medium-treated C2C12 myotubes than in non-tumor medium-treated C2C12 myotubes (Figure 5C). Similarly, the levels of miR-195a-5p and miR-125b-1-3p were significantly higher in C26 exosome-treated C2C12 myotubes than in MC38 exosome-treated C2C12 myotubes (Figure 5D). The abundance of miR-195a-5p and miR-125b-1-3p in serum and GA tissue of C26 tumor-bearing mice was significantly higher than those of healthy mice (Figure 5E). Similar results were found in TA tissue with high dose of C26 exosome intramuscular injection (Figure 5F). To investigate whether miR-195a-5p and miR-125b-1-3p were active in inducing skeletal muscle atrophy, mimics of miR-195a-5p or miR-125b-1-3p were transfected into C2C12 myotubes (Figure S5). As shown in Figures 5G–5I, miR-195a-5p mimic or miR-125b-1-3p mimic could induce atrophy of C2C12 myotubes and significantly decreased the diameter of C2C12 myotubes and the level of MHC protein in the C2C12 cells, which were more significant with the two miRNA mimics. Inhibitors of miR-195a-5p and miR-125b-1-3p could alleviate the decrease of C2C12 myotube diameter induced by C26 exosomes (Figure S6). These results demonstrated that miR-195a-5p and miR-125b-1-3p might be the active components in C26 exosomes that could induce skeletal muscle atrophy.

C26 exosomal miRNAs mediate skeletal muscle atrophy by activating apoptotic signaling

It is known that miRNAs can participate in physiological and pathological progression by regulating the expression of target genes. To

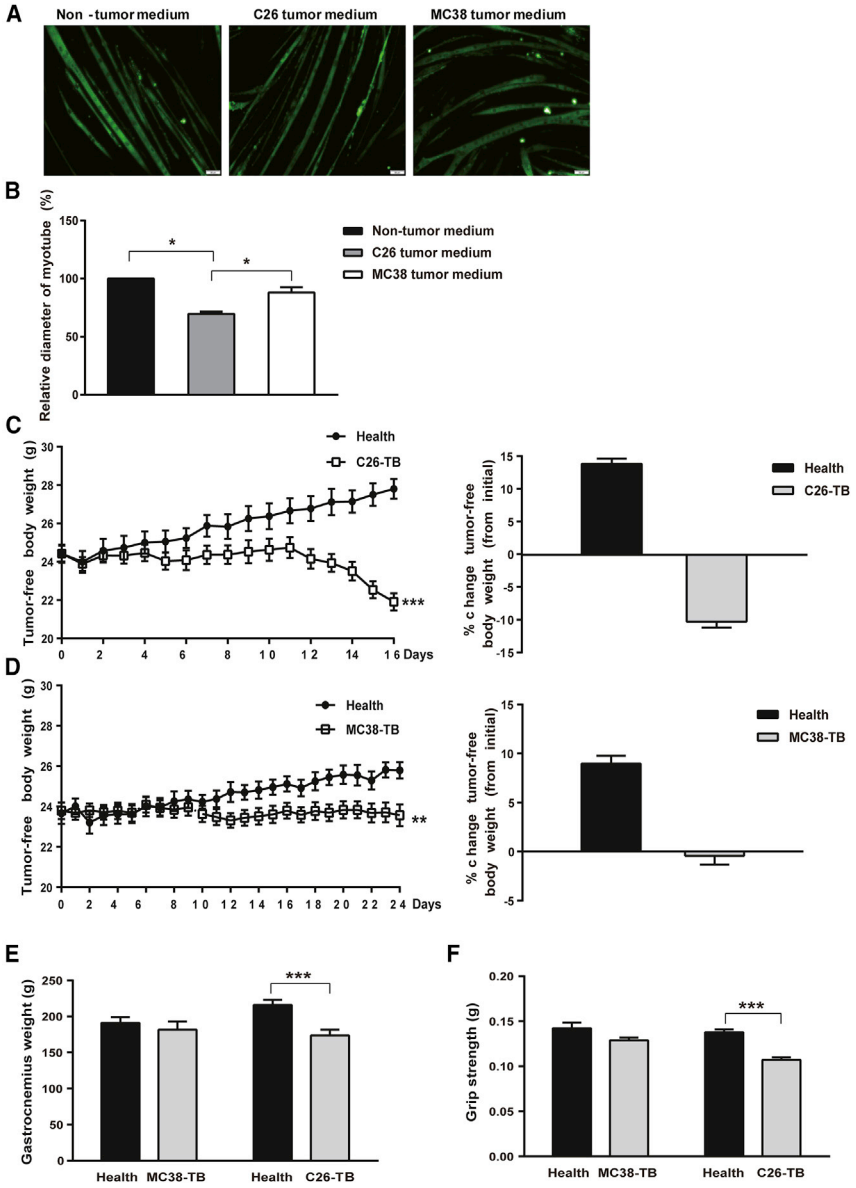

Figure 2. C26 but not MC38 tumor cells induce skeletal muscle wasting *in vitro* and *in vivo*

(A) Non-tumor medium (3T3-L1 cell medium), C26 tumor medium, and MC38 tumor medium (1:1 dilution with fresh normal medium) were incubated with C2C12 myotubes for 48 h. Immunofluorescent staining (green) for C2C12 myotubes (scale bars, 50 μm). (B) Quantified diameter of myotubes of (A). (C and D) Profiles of the time-related change in tumor-free body weight of mice inoculated with C26 tumor cells (C) or MC38 tumor cells (D) and percentage of change in the tumor-free body weight of C26-inoculated mice (C) from day 0 to day 16 or MC38-inoculated mice (D) from day 0 to day 24. (E) GA weight of C26-inoculated mice or MC38-inoculated mice. (F) Grip strength of C26-inoculated mice or MC38-inoculated mice. Data presented are the mean ± SEM of three independent experiments. *p < 0.05, **p < 0.01, **p < 0.001.

identify the possible target genes of miR-195a-5p and miR-125b-1-3p, we combined bioinformatics analysis and literature investigation and found a candidate gene, *bcl2*, encoding an apoptosis inhibitor protein (Figure 6A). Results of dual-luciferase assay confirmed the targeting of miR-195a-5p/miR-125b-1-3p to Bcl-2 (Figure 6B). Both the mRNA level (Figure 6C) and protein level (Figure 6D) of Bcl-2 were downregulated in C2C12 myotubes transfected with miR-195a-5p mimic or miR-125b-1-3p mimic, and the decrease of Bcl-2 protein expression was more significant with the two miRNA mimics (Figure 5I). The activation of the apoptotic signaling pathway such as cleavage of caspase-3 was observed in miRNA mimic-treated C2C12 myotubes, while the activation of the ubiquitination pathway (indicated by the level of MuRF-1) was not obvious (Figure 6D). TUNEL assay also showed that the apoptotic rate of TA muscle injected with a high dose of C26 exosomes was significantly higher than that of the control group (Figures 6E and 6F). Western blot assays found that the expression of BCL-2 was significantly downregulated in the high-dose group but the ubiquitination pathway was barely affected (Figure 6G). What is more, the apoptosis rate in GA muscle of C26 tumor-bearing mice was significantly higher than that of the healthy mice (Figures S7A and S7B). Western blot assays showed that the expression of BCL-2 was downregulated and the apoptotic signaling pathway was activated in the myocytes of C26 tumor-bearing mice (Figure S7C). Results showed that apoptosis pathway could contribute to muscle wasting in addition to the ubiquitination-proteasome pathway. Furthermore, overexpression of Bcl-2 successfully reversed C2C12 atrophy induced by miR-195a-5p mimic and miR-125b-1-3p mimic (Figure 7; Figure S8). These results suggested that C26 exosomal miRNAs (miR-195a-5p and miR-125b-1-3p) could induce skeletal muscle atrophy by regulating the apoptotic signaling pathway.

DISCUSSION

Cancer cachexia, characterized by severe wasting of muscle, contributes to high mortality rate of cancer patients, especially for advanced solid tumor. It is believed that cancer cachexia is responsible for the death of >20% of cancer patients directly and indirectly.[27] It is known that cancer cells can secrete a large number of vesicles including exosomes in the process of proliferation.[28–30] Cancer exosomes, via containing active components, may have a wide range of regulatory roles in the development of cancer cachexia. In the present study, we observed the role of cancer exosomes and their active miRNAs in

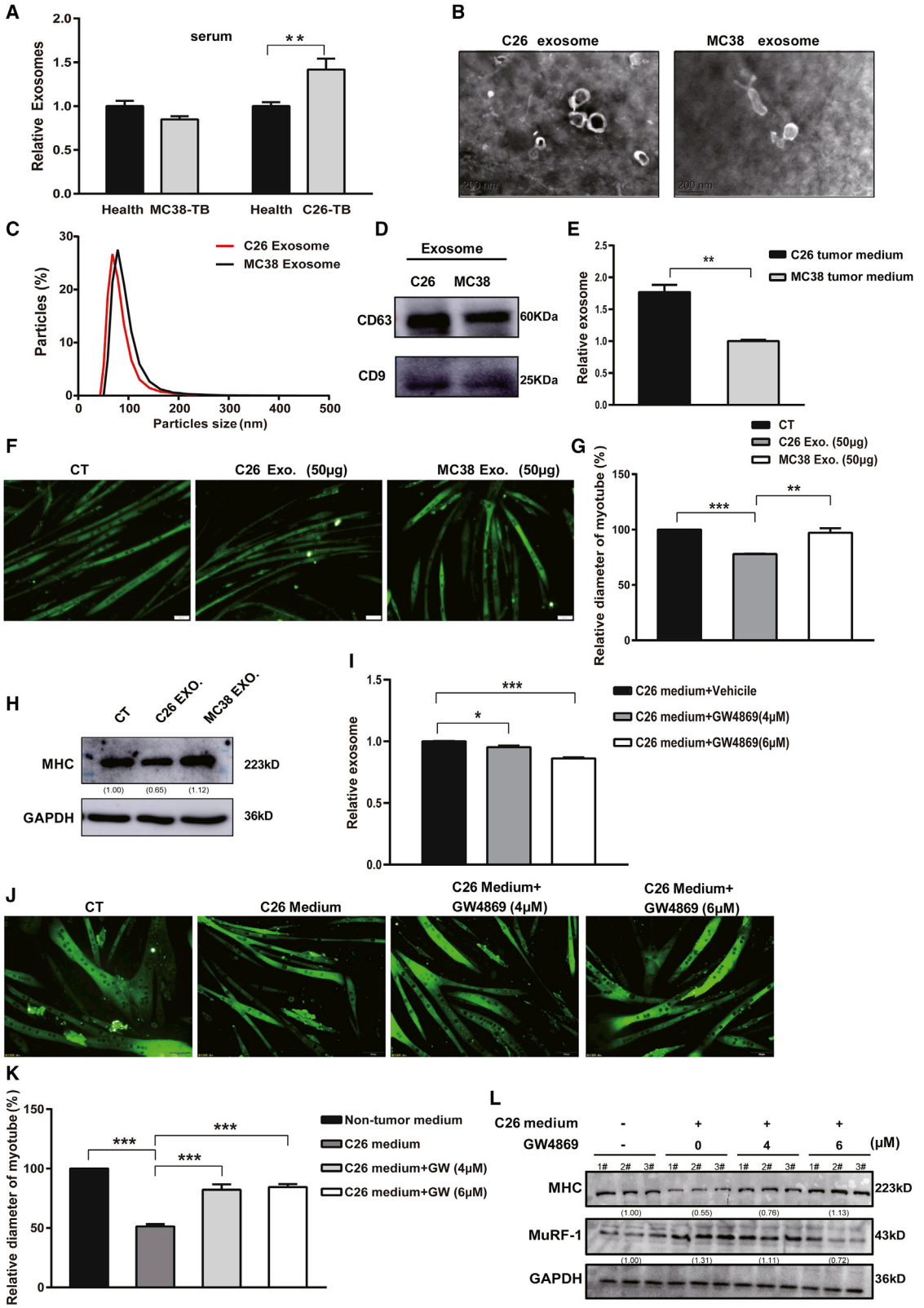

(legend on next page)

development of colon cancer cachexia to try to clarify the possible mechanisms of cancer exosomes in induction of muscle atrophy.

The involvement of exosomes in development of colon cancer cachexia was observed by analyzing clinical samples as well as the samples from an *in vivo* animal study and an *in vitro* cell culture study. Results of comparison of the exosome concentrations in serum of healthy persons and colon cancer patients with or without cachexia suggested that exosomes were closely related to colon cancer cachexia. The serum exosome concentration in cachexia patients was significantly higher than that in non-cachexia patients. Similar results were observed in an *in vivo* animal study comparing the serum of mice bearing cachectic C26 tumor and mice bearing non-cachectic MC38 tumor as well as in an *in vitro* study comparing the culture medium of C26 tumor cells and that of MC38 tumor cells. It is known that C26 colon cancer cells can induce cancer cachexia, skeletal muscle atrophy, and lipolysis *in vitro* and *in vivo*, which is a classic model for studying cancer cachexia. By comparison, MC38 colon cancer cells can not induce cachexia *in vitro* and *in vivo* and thus are considered a kind of non-cachectic cell line.[22] Our results also confirmed that inoculation of C26 tumor cells induced obvious cancer cachexia symptoms in C26 tumor-bearing mice (loss weight of body and GA tissue, hypothermia, etc.) whereas inoculation of MC38 tumor cells did not induce cancer cachexia symptoms in MC38 tumor-bearing mice. Importantly, the serum exosome concentration of C26 tumor-bearing mice was significantly higher than that of the healthy group, whereas there was no difference between the serum exosome concentration of MC38 tumor-bearing mice and the healthy group. In a cell culture study, culture medium of C26 cells could induce atrophy of C2C12 myotubes, whereas culture medium of MC38 cells could not. Furthermore, exosome concentration in the C26 culture medium was significantly higher than that in the MC38 culture medium. These results suggested the involvement of cancer exosomes in inducing muscle atrophy in colon cancer cachexia. Our results were in accordance with a previous report that showed that cancer cachexia was associated with elevated circulating extracellular vesicles (EVs) (including exosomes) in mice bearing Lewis lung carcinoma (LLC) cells.[31] It is interesting that the role of exosomes in regulating cancer cachexia is beginning to unravel in recent times.[9,10]

Direct inducing effects of C26 exosomes on muscle atrophy were observed in the present study. C26 exosomes could be successfully absorbed by cultured C2C12 myotubes and dose-dependently induced C2C12 myotube atrophy, as indicated by the decrease in the diameter of myotubes and the protein expression level of MHC. Furthermore, intramuscular injection of C26 exosomes could significantly decrease the muscle strength and the weight of the TA muscle. These results suggested that C26 exosomes could directly induce skeletal muscle atrophy *in vitro* and *in vivo*. The roles of C26 exosomes in inducing muscle atrophy were further confirmed in an *in vivo* study by blocking exosome production with the exosome secretion inhibitor GW4869. GW4869 treatment in C26 tumor-bearing mice effectively alleviated the loss in TA muscle weight and the weakening of TA grip strength. Moreover, GW4869 treatment of C26 tumor cells was effective in inhibiting the ability of C26 culture medium to induce atrophy of C2C12 myotubes *in vitro*, compared with non-treated C26 cells. Interestingly, Yang et al. have also shown that knockdown of ZIP4 in pancreatic cancer cells could inhibit extracellular vesicle release and thus ameliorate muscle wasting in mice, as indicated by higher muscle mass, decreased protein degradation, and preserved myofiber cross-sectional area.[32] These results suggested that exosomes play an important role in development of cancer cachexia and that inhibition of exosome production would ameliorate muscle atrophy in cancer cachexia. The muscle wasting in cancer cachexia might be caused by various tumor-derived signaling factors including exosomes. In other words, cancer exosomes have the ability to directly induce muscle atrophy.

Exosome enriched proteins, lipids, and nucleic acids can participate in the biological process of cancer cachexia in many ways, including the regulation of skeletal muscle wasting. In the present study, we concentrated on searching the active miRNAs in C26 exosomes with atrophy-inducing effects on muscle cells. Previous reports showed that microvesicles containing miRNA-21 promoted muscle cell death in cancer cachexia via TLR7 and JNK signaling pathway.[18] The transfer of miR-155 from exosomes acts as an oncogenic signal reprogramming systemic energy metabolism and leading to cancer-associated cachexia in breast cancer.[33] miR-26a limits muscle wasting through exosome-mediated miRNA transfer in chronic kidney induced cachexia.[19,20] By comparing miRNA profiles of C26 exosomes and MC38 exosomes with miRNA-seq analysis, and further confirming by RT-PCR assay, two miRNAs (miR-195a-5p and miR-125b-1-3p) were found to exhibit high levels in C26 exosomes. In line with this, the levels of miR-195a-5p and miR-125b-1-3p were significantly higher in C2C12 myotubes treated with C26 exosomes than in C2C12 myotubes treated with MC38 exosomes. Furthermore, the abundance of miR-195a-5p and miR-125b-1-3p in serum and GA of C26 tumor-bearing mice was significantly higher than those of healthy mice. Similar results were found in TA with high doses of C26 exosome intramuscular injection. Notably, transfection

Figure 3. C26 tumor-derived exosomes induced skeletal muscle atrophy *in vitro*

(A) The content of exosomes in serum of C26-inoculated mice or MC38-inoculated mice. (B) Electron microscopy images of exosomes isolated from C26 medium or MC38 medium (scale bars, 200 nm). (C) Particle size analysis of exosomes isolated from C26 medium or MC38 medium. (D) Western blot analysis showed the expression of exosomal biomarkers in C26 cell and MC38 cell exosomes. (E) Exosomes in C26 culture medium or MC38 culture medium were detected by AchE Assay Kit. (F) The C2C12 myotube atrophy induced by exosomes (scale bars, 50 μm). (G) Quantified diameter of myotubes of (F). (H) MHC expression was measured by western blot analysis. (I) The content of exosomes in C26-conditioned medium treated with vehicle or GW4869. (J) Treatment function of GW4869 on C2C12 myotube atrophy (scale bars,50 μm). (K) Quantified diameter of myotubes of (J). (L) MHC and MuRF-1 expression was measured by western blot analysis. Data presented are the mean ± SEM of three independent experiments. $^{**}p < 0.05$, $^{**}p < 0.01$, $^{***}p < 0.001$.

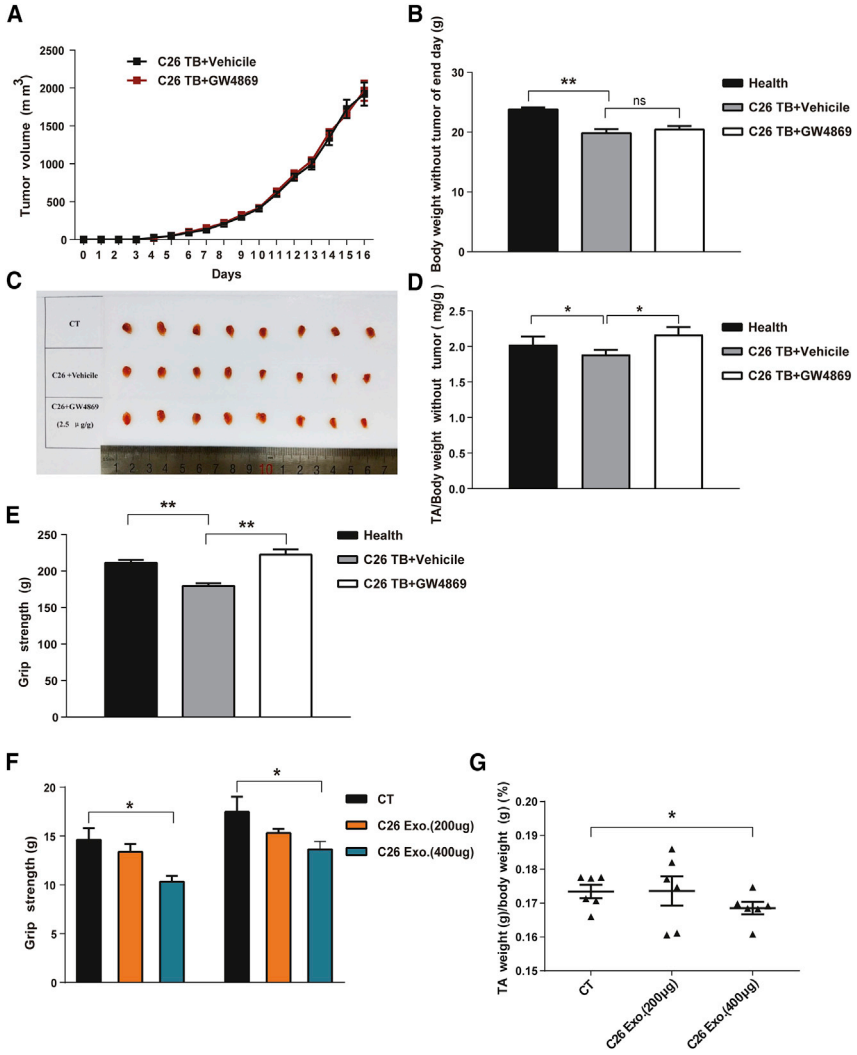

Figure 4. C26 tumor-derived exosomes induce skeletal muscle wasting *in vivo*

(A) Time-related tumor growth curve in mice inoculated with C26 tumor treated with vehicle (PBS) or GW4869 (intratumoral injection). (B) Tumor-free body weight of healthy mice and C26-inoculated mice treated with vehicle or GW4869 at the end of the experiment. (C) Photo of TA tissue (healthy mice and C26-inoculated mice treated with vehicle or GW4869) isolated from mice at the end of the experiment. (D) Relative weight of TA tissues at the end of the experiment. (E) Grip strength of healthy mice and C26-inoculated mice treated with vehicle or GW4869. Healthy mice with intramuscular injection of C26 exosomes into the TA of the left hindlimb. (F) Grip strength of healthy mice and C26 exosome intramuscular injection mice on day 10 and on day 22. (G) Relative weight of TA tissue at the end of the experiment. Data presented are the mean ± SEM of three independent experiments. *p < 0.05, **p < 0.01.

of mimics of miR-195a-5p or miR-125b-1-3p could induce atrophy in C2C12 myotubes. These results demonstrated that C26 exosomal miR-195a-5p and miR-125b-1-3p might be active components mediating skeletal muscle atrophy during cancer cachexia.

A further study clarifying the mechanisms of miR-195a-5p and miR-125b-1-3p in inducing muscle atrophy suggested that bcl-2 might be the target gene of the two miRNAs in muscle cells. Results of dual-luciferase assay confirmed the targeting of miR-195a-5p/miR-125b-1-3p to bcl-2, and both the mRNA expression level and protein expression level of bcl-2 were downregulated in C2C12 myotubes transfected with miR-195a-5p mimic or miR-125b-1-3p mimic. The activation of the apoptotic signaling pathway such as cleavage of caspase-3 was observed in miRNA mimic-treated C2C12 myotubes. Furthermore, the expression of BCL-2 was downregulated and the apoptosis rate in muscle of C26 tumor-bearing mice was significantly higher than that of the healthy mice. The apoptotic rate of muscle injected with C26 exosomes was also significantly higher than that of the control group. Importantly, overexpression of bcl-2 successfully reversed C2C12 atrophy induced by miR-195a-5p mimic or miR-125b-1-3p mimic. These results suggested that C26 exosomal miRNAs (miR-195a-5p and miR-125b-1-3p) might induce skeletal muscle atrophy by targeting bcl-2 and regulating the apoptotic signaling pathway.

Previous studies also reported that miR-195a-5p and miR-125b-1-3p targeted bcl-2 and influenced the apoptosis signal pathway in other kinds of cells. For example, Yang et al. reported that miR-125b enhanced chemotherapy sensitivity to cisplatin by downregulating Bcl-2 in gallbladder cancer.[34] In mouse podocytes, miR-195 promotes apoptosis via enhanced caspase activity driven by BCL-2 insufficiency.[35] These studies showed that miR-195 and miR-125b could regulate bcl-2 and apoptotic signaling. Our results further confirmed that miR-195a-5p and miR-125b-1-3p in C26 exosomes could induce myo-atrophy by targeting bcl-2 to activate myotubular cell apoptosis.

Muscle atrophy is mainly caused by the enhancement of protein degradation. The apoptosis pathway is one of the pathways that contribute to protein degradation in muscle atrophy, besides the ubiquitin-proteasome pathway and the autophagy-lysosome pathway.[5,9] Apoptosis could be activated during cachexia of humans and mice. Sílvia Busquets et al. found that apoptosis is present in skeletal muscle of cachectic gastro-intestinal cancer patients.[4,5] Apoptosis markers were observed in severely cachectic muscle of Apc (Min/+) mice.[6] In addition, catalpol alleviates denervated muscular atrophy through reducing BAX-to-BCL2 ratio and autophagy via the mTOR signaling pathway.[36] PGC1β overexpression

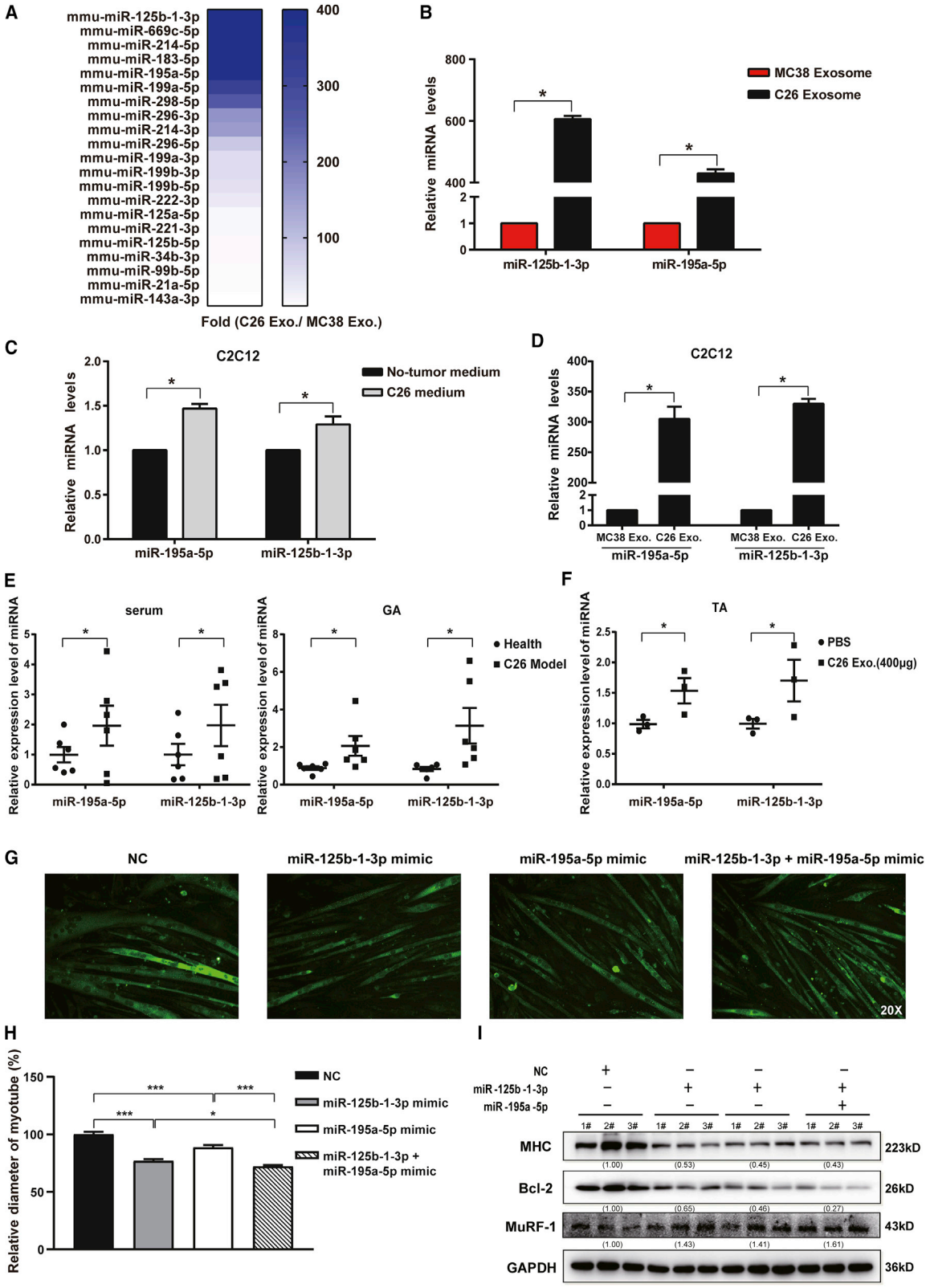

(legend on next page)

could activate apoptosis signaling to promote skeletal muscle wasting.[35] Lack of caspase-3 attenuates immobilization-induced muscle atrophy and loss of tension generation along with mitigation of apoptosis and inflammation.[37] FoxO1 induces apoptosis in skeletal myotubes in a DNA-binding-dependent manner.[38] Dulaglutide acts on disuse muscle atrophy through inhibition of inflammation and apoptosis by induction of Hsp72 expression.[39] SNARK-mutant LLC-bearing mice had increased skeletal muscle BAX protein expression, a marker of apoptosis, compared with other groups.[40] What is more, miRNAs could participate in the regulation of apoptotic signaling pathways during cachexia. In addition to miR-21 and miR-26a mentioned earlier, miR-628 promotes burn-induced skeletal muscle atrophy via targeting IRS1 by influencing apoptosis.[41] miR-142a-5p was able to function as an important regulator of denervation-induced skeletal muscle atrophy by inducing apoptosis via targeting MFN1.[42] In conclusion, the miRNA-mediated apoptosis signaling pathway plays an important role in skeletal muscle wasting. In this study, we found that miR-195a-5p and miR-125b-1-3p promoted skeletal muscle atrophy by regulating the apoptotic signal pathway rather than the MuRF-1-related ubiquitination pathway. Bcl-2 and the apoptosis signaling pathway might play an important role in the process of skeletal muscle atrophy in cancer cachexia.

In summary, we demonstrate in the present study that exosomes might be involved in the development of colon cancer cachexia in the clinic and that C26 cancer exosomes play an important role in development of muscle atrophy in cancer cachexia both *in vitro* and *in vivo*. In addition, we show that miR-195a-5p and miR-125b-1-3p might be active components in C26 exosomes with atrophy-inducing effects on muscle cells. Further, we report that the bcl-2 gene and its downstream apoptosis signaling are the target gene and signal pathway of C26 exosomal miR-195a-5p and miR-125b-1-3p. These findings suggest that Bcl-2-mediated apoptosis might be the main target of tumor-released exosome miRNAs such as miR-195a-5p and miR-125b-1-3p in inducing muscle wasting of colon cancer cachexia.

MATERIALS AND METHODS

Reagents and antibodies

RIPA lysis buffer, extraction buffer, and Halt Protease and Phosphatase Inhibitor Cocktail (100×) were purchased from Thermo Scientific and stored at 4°C. BCA protein assay kits used to quantify protein concentration were purchased from Beyotime and stored at room temperature. DMEM (High Glucose), RPMI1640, penicillin-streptomycin, and trypsin-EDTA were purchased from HyClone. Horse serum was purchased from Gibco. Fetal bovine serum (FBS) was derived from Biological Industries. miRNA qPCR primer and miRNA mimic (RiboBio), GW4869 (MCE), PEG8000 (Sigma-Aldrich), PKH67 Green Fluorescent Cell Linker Kit (Sigma), Oligofectamine (Invitrogen), X-tremeGENE 9 (Roche), TRIzol (Vazyme), T4 DNA ligase (Takara), DH5α-competent cells (TIAGEN), SYBR Green (Takara), miRNA mimic (RiboBio), Direct-zol RNA Miniprep (Zymo), and the Dual-Luciferase Reporter Assay System (Promega) were used. Other chemicals, except where specially noted, were purchased from Sigma-Aldrich.

Clinical serum samples

A total of 40 serum samples were collected from healthy persons (19 cases) and non-cachexia (13 cases) and cachexia (8 cases) patients with colon cancer at Shanghai Tenth People's Hospital, Tongji University School of Medicine between January 2014 and January 2019. The study was examined and approved by the Ethics Committee of the Shanghai Tenth People's Hospital, Tongji University School of Medicine (approval no: SHSY-IEC-pap-16-24). This study was registered with ClinicalTrials.gov (ClinicalTrials.gov: NCT02917707). All of the serum samples were immediately frozen and stored at −80°C until use.

Cell culture

C26 cells and MC38 cells, obtained from Shanghai Institute of Materia Medica, Chinese Academy of Sciences, were maintained in RMPI-1640 medium containing 10% FBS at 37°C with 5% CO_2. The C2C12 murine myoblast cell line, obtained from ATCC, was cultured in high-glucose DMEM with 10% FBS at 37°C with 5% CO_2. During differentiation, the medium of cells planted on culture plates coated with 0.1% gelatin was switched to differentiation medium (high-glucose DMEM containing 2% horse serum) when cell confluence reached 70%. After 5 days, multinuclear myotubes were formed. 3T3-L1 cells, obtained from Shanghai Institute of Materia Medica, Chinese Academy of Sciences, were cultured in high-glucose DMEM with 10% FBS at 37°C with 5% CO_2. All cells were negative for mycoplasma contamination before use.

C26 tumor medium collection

When C26 or MC38 tumor cell confluence reached 70%, the medium was switched to new high-glucose DMEM medium for 48 h. Thereafter, medium was collected and centrifuged at 1,000 × *g* for 5 min, then centrifuged at 10,000 × *g* for 10 min. Medium from non-tumor cells (3T3-L1 cells) was used as control medium. The final supernatant was filtered and stored at −20°C or used immediately at a 1:1 dilution with fresh normal medium.

Figure 5. C26 exosomal miRNA regulates skeletal muscle atrophy

(A) miRNA differences between C26 exosomes and MC38 exosomes by miRNA-seq analysis. (B) The expression of miR-125b-1-3p and miR-195a-5p in C26 and MC38 exosomes was measured by real-time qPCR analysis. (C) Relative miRNA expression of C2C12 myotubes treated with C26 tumor medium. (D) Relative miRNA expression of C2C12 myotubes treated with C26 exosomes and MC38 exosomes. (E) Relative miRNA expression in serum or GA tissues of C26 tumor-bearing mice. (F) Relative miRNA expression in TA tissues treated with C26 exosome by intramuscular injection. (G) The C2C12 myotube atrophy was induced by miR-125b-1-3p mimic and miR-195a-5p mimic (20×). (H) Quantified diameter of myotubes of (G). (I) MHC, Bcl-2, and MuRF-1 expression was measured by western blot analysis. Data presented are the mean ± SEM of three independent experiments. *$p < 0.05$, **$p < 0.01$, **$p < 0.01$.

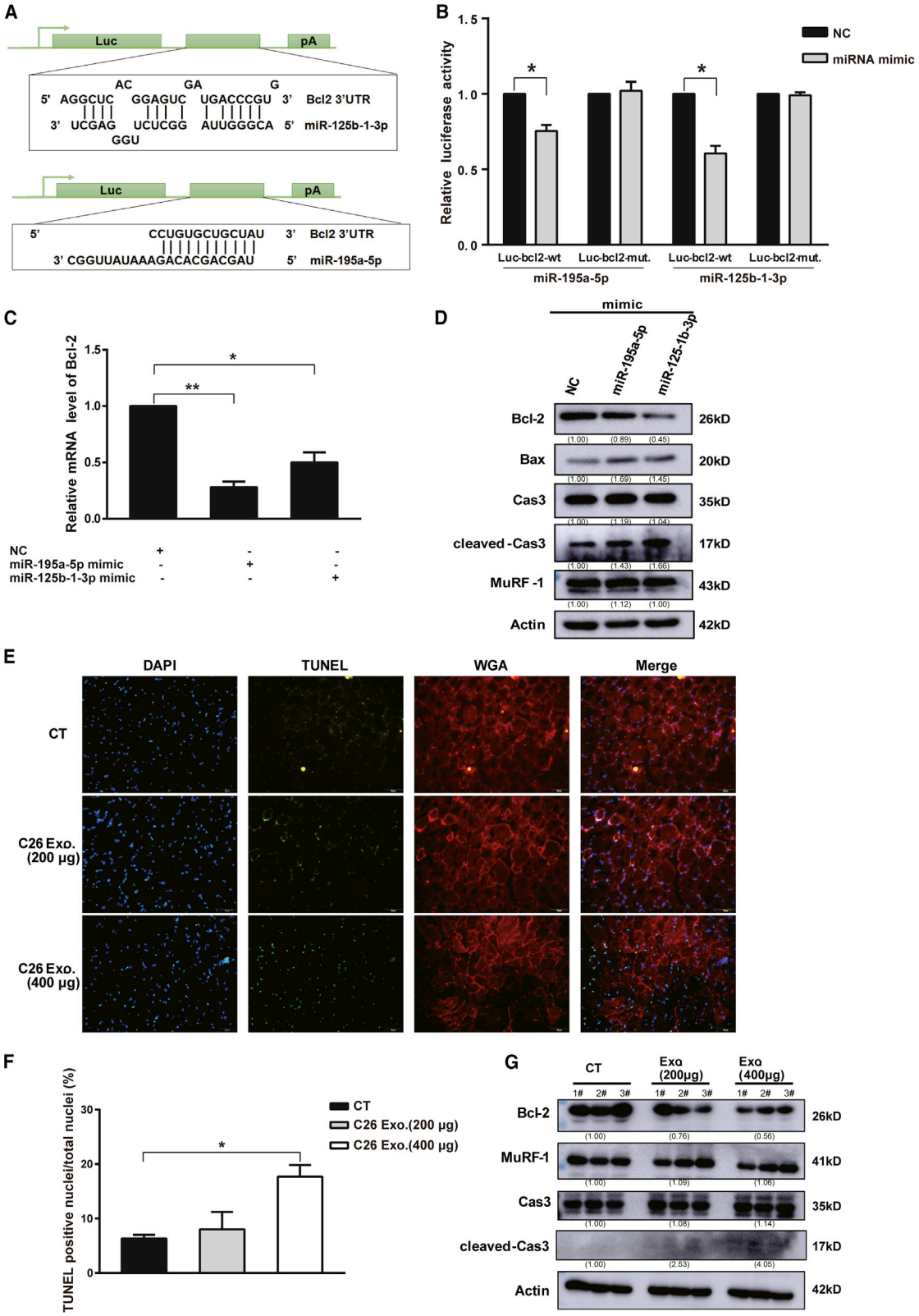

(legend on next page)

Exosome purification

Exosomes were extracted from conditioned medium of cells, mouse serum, or human serum with ExoQuick-TC Exosome Isolation Reagent (SBI, EXOTC10A-1) according to the manufacturer's protocol. In brief, culture supernatants were collected and centrifuged at 1,500 × *g* for 5 min to pellet dead cells and cell debris. The ~5 mL supernatant was then mixed with 1 mL of ExoQuick-TC reagent mix by inverting 4 times. The mixture was incubated at 4°C overnight and centrifuged at 1,500 × *g* for 30 min at 4°C to pellet the exosomes. The pelleted exosomes were resuspended with phosphate-buffered saline (PBS) and quantified with a BCA Protein Assay Kit (T9300A; Takara, China).

Exosome detection

Isolated EVs were quantified by measuring the activity of AchE according to the Amplex Red Acetylcholine/Acetylcholinesterase Assay Kit (Invitrogen, A12217). Briefly, isolated EV preparations were suspended in 120 μL of PBS and diluted with 120 μL of reaction buffer. One hundred microliters of the diluted samples and controls were pipetted into separate wells of a microplate. The reactions were started by adding 100 μL of the Amplex Red reagent/horseradish peroxidase (HRP)/choline oxidase/acetylcholine working solution to each microplate well containing the samples and controls. The reactions were incubated for 30 min or longer at room temperature, protected from light. The fluorescence was measured in a fluorescence microplate reader using excitation in the range of 530–560 nm and emission detection at ~590 nm.

Transmission electron microscopy

Exosome pellets were fixed in 2% paraformaldehyde (PFA) for 30 min and resuspended with 100 μL of PBS. The suspension was added to the copper grids for 20 min in a dry environment. Grids were immersed in the glutaraldehyde for 5 min and washed with fresh water. Then grids were immersed in the neutral uranium oxalate dioxide solution for 5 min, followed by methyl cellulose uranyl acetate for 10 min, and grids were allowed to dry. Samples were then examined under a JEM-1010 electron microscope (Jeol, Tokyo, Japan).

Exosome particle size analysis

Exosome pellets were resuspended with 1 mL of PBS and subjected to particle size analysis using the Zetasizer Nano S90 system.

Exosome tracing

For exosome tracing experiments, C26-derived exosomes were labeled with the PKH67 Green Fluorescent Cell Linker Kit (Sigma-Aldrich) according to the manufacturer's protocol. Exosomes diluted in PBS were added to 1 mL of Diluent C within 4 mL of PKH67 dye and incubated for 4 min. To bind excess dye, 2 mL of 0.5% bovine serum albumin (BSA) was added. The labeled exosomes were extracted by ExoQuick-TC Exosome Isolation Reagent, and the exosome pellet was diluted in 100 μL of PBS and used for tracing experiments. C2C12 myotubes were treated with 50 μg of PKH67-labeled C26 exosomes for 12 h at 37°C and imaged with a fluorescence microscope (Leica).

Animals and cancer cachexia mouse model

All animal (purchased from Shanghai SLAC Laboratory Animal, Co., Ltd., Shanghai, China) care and experimental protocols for this study complied with Chinese regulations and the *Guide for the Care and Use of Laboratory Animals* drawn up by the National Institutes of Health (United States) and were approved by the Institutional Animal Care and Use Committee of the East China Normal University. Male BALB/c mice (6–8 weeks) and C57BL/6 mice were purchased from the Shanghai SLAC Laboratory Animal. Mice were maintained on a 12:12-h light-dark cycle in a temperature-controlled (21~23°C) and specific pathogen-free (SPF) conditional room and were provided standard rodent chow and water *ad libitum*. All animals were acclimatized for a week before beginning the study.

Male BALB/c mice were randomly divided into two groups (n = 8): the healthy group (without tumor) and the C26 tumor-bearing mouse group (C26 TB). On day 0, mice were implanted subcutaneously in the right flank with 100 μL (1.0×10^6) of C26 cells. C57BL/6 mice were randomly divided into two groups: the healthy group (without tumor, n = 7) and the MC38 tumor-bearing mouse group (MC38 TB, n = 8). On day 0, mice were implanted subcutaneously in the right flank with 100 μL (2.0×10^6) of MC38 cells. Body weight, tumor volume, and body temperature were measured daily from inoculation to completion of the study. The shortest diameter (X) and longest diameter (Y) of tumor were recorded with calipers. Tumor volume was calculated following the formula $V = X \times X \times Y \times 0.5$. We summarized the data (volume and weight of tumor) obtained from many experiments and found that the density of tumor was ~1 g/1,000 mm^3. Based on this, we calculated the tumor weight during the growth of the tumor and then obtained the body weight without tumor of mice. When the mice lost 10% of their body weight or when their tumor volumes reached 2,000 mm^3, the experiment was terminated. The GA muscle tissues of mice were rapidly dissected, weighed, and frozen in liquid nitrogen and then stored at −80°C until ready for further analyses or fixed in 4% PFA overnight and embedded in paraffin.

Figure 6. C26 exosomal miRNA mediates skeletal muscle atrophy by activating the apoptotic signaling

(A) Prediction of the miR-125b-1-3p and miR-195a-5p target gene. (B) The luciferase expression level of 293T cells transfected with bcl2 wild-type 3′ UTR vector (WT) or mutant 3′ UTR vector (mut, miR-125b-1-3p and miR-195a-5p target sites were mutated) and miR-125b-1-3p or miR-195a-5p mimic. (C) Relative bcl2 mRNA expression of C2C12 myotubes transfected with miR-125b-1-3p or miR-195a-5p mimic. (D) Representative western blot of Bcl2, Bax, MuRF-1, Caspase3, and cleaved-Caspase3 in C2C12 myotubes transfected with miR-125b-1-3p or miR-195a-5p mimic. (E and F) Apoptosis detection with TUNEL staining in TA tissues of intramuscular injection with PBS or C26 exosomes (DAPI, blue; TUNEL, green; WGA, red; scale bars, 50 μm). (G) Representative western blot of Bcl2, Bax, Caspase3, and cleaved-Caspase3 in TA tissues of intramuscular injection with PBS or C26 exosomes (three mice per group). Data presented are the mean ± SEM of three independent experiments. $^*p < 0.05$, $^{**}p < 0.01$.

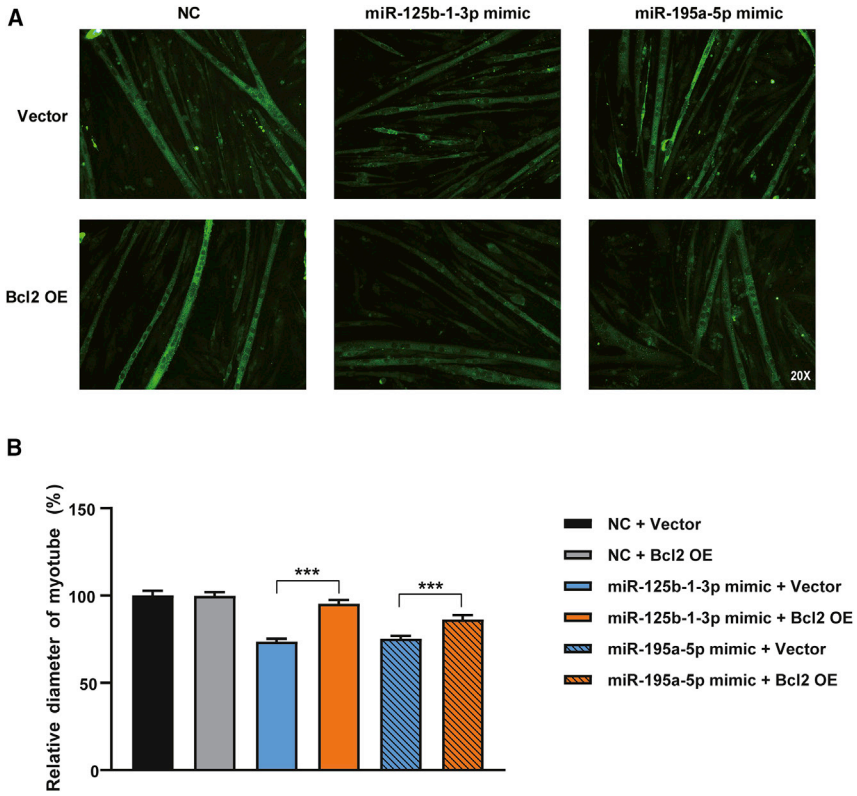

Figure 7. Overexpression of Bcl-2 reverses C26 exosomal miRNA inducing skeletal muscle atrophy

(A) Immunofluorescent staining for C2C12 myotubes (20×). (B) Quantified diameter of myotubes of (A). Data presented are the mean ± SEM of three independent experiments. ***$p < 0.01$.

GW4869 drug administration

Male BALB/c mice with the same initial body weight were randomly divided into three groups (8 mice per group): the healthy group (without tumor), the Colon-26 tumor-bearing mouse group (C26 model group), and the C26 tumor-bearing mouse treated with GW4869 group. On day 0, mice were implanted subcutaneously in the right flank with 100 μL (1×10^6) of C26 colon adenocarcinoma cells. Starting from the next day, C26 model group mice received a single intra-tumor injection of sterile saline every other day, while GW4869-treated group mice received single intra-tumor injections of GW4869 (2.5 μg/g tumor/25 μL) every other day. Body weight, tumor volume, and food intake were measured daily from inoculation to completion of the study. The shortest diameter (X) and longest diameter (Y) of tumor were recorded with calipers every day. Tumor volume was calculated following the formula V = XxXxYx0.5. When the mice lost 10% of their body weight or when their tumor volumes reached 2,000 mm^3, mice were euthanized by CO_2 inhalation and tumor and GA muscle tissues were rapidly dissected, weighed, and frozen in liquid nitrogen and then stored at −80°C until ready for further analyses or fixed in 4% PFA overnight for future analysis.

Intramuscular injection of C26 exosomes

Male BALB/c mice were randomly divided into three groups (6 mice per group): the healthy group, the C26 Exo (1×, 200 μg/mice) group, and the C26 Exo (2×, 400 μg/mice) group. Exosomes (50 μL) were injected into the TA muscle of the left hindlimb, and the healthy group received only with the same amount of PBS once a day for 22 days. Body weight was measured daily until the completion of the study. The grip strength of left hindlimbs was measured at day 10 and day 22. At the end of the study, serum was collected from mouse orbit for biochemistry test, and TA muscles were dissected rapidly, weighed, and fixed in 4% PFA for future analysis.

Western blot analysis

Western blots were performed as described previously.[43] Briefly, C2C12 myotubes were homogenized in RIPA buffer plus a phosphatase protease inhibitor. The lysates were centrifuged at 13,000 rpm for 30 min at 4°C. The supernatant was quantified for protein concentration with the BCA Protein Assay Kit (Beyotime). Equal amounts of protein samples were separated by 10% SDS-PAGE gel electrophoresis and transferred to a polyvinylidene fluoride (PVDF) membrane. The PVDF membranes were blocked in 5% non-fat milk in PBS containing 0.1% Tween 20 (PBST) for 1 h at room temperature and then incubated with primary antibodies diluted in 5% BSA-TPBS at 4°C overnight. The primary antibodies used were as follows: MuRF-1 (Proteintech), MHC (DSHB), CD9 (ABclonal), CD63 (ABclonal), Bcl2 (ABclonal), Bax (Cell Signaling Technology), Caspase3 (ABclonal), and GAPDH-HRP (Santa). Anti-mouse (Multi Sciences) and anti-rabbit (Multi Sciences) IgG HRP-conjugated secondary antibodies were incubated with membranes for 1 h in 5% non-fat milk in TPBS. The ECL Chemiluminescent Kit (Thermo Fisher) was used to visualize the antibody-antigen interaction, and chemical luminescence of membranes was detected by an Amersham Imager 600 (GE).

miRNA-seq analysis

miRNAs contained in C26-derived and MC38-derived exosomes were determined by the Illumina HiSeq platform. High-throughput sequencing was conducted at Shanghai Majorbio Biopharm Technology Co., Ltd. (Shanghai, China). In brief, total RNA from exosomes was prepared and quantified with a NanoDrop ND-2000 (NanoDrop Technologies). RNA integrity was assessed with a 2100 Bioanalyzer (Agilent Technologies, Santa Clara, CA, USA). A total amount of 3 μg of total RNA per sample was used as input material for the small RNA library. Small RNA adapters were then ligated to the 5′ and 3′ ends of total RNA. After cDNA synthesis and amplification, the PCR-amplified fragments were purified from the PAGE gel, and the

completed cDNA libraries were quantified by an Agilent 2100 Bioanalyzer. Cluster generation was performed on an Illumina cBot, sequencing was performed on an Illumina HiSeq 2000 platform, and 50 bp single-end reads were generated. The expression level of each miRNA was calculated according to the transcripts per million reads (TPM) method. Significant differently expressed (DE) miRNAs were extracted with |log2 fold change (FC)| >1 and false discovery rate (FDR) <0.05 by DEseq2.

Quantitative RT-PCR

Total RNA extraction was performed with the RNeasy Mini Kit (QIAGEN) according to the manufacturer's instructions. The Bulge-Loop miRNA qPCR Primer Set (RiboBio) was used to determine the expression levels of miRNAs by qRT-PCRs in a Bio-Rad CFX96 Real-Time PCR Detection System. U6 was used as an internal control. All the relative expression level of miRNA was calculated with the $2^{-\triangle\triangle Ct}$ method.

miRNA mimic transfection

A mixture of 1.25 μL of miRNA mimic (final concentration 50 nM) and 50 μL of Opti-MEM was labeled A, and a mixture of 1.25 mL of Oligofectamine and 50 μL of Opti-MEM was labeled B. Make sure A and B mixed fully and static 20 min. Then add them to the cell conditioned medium drop by drop slowly. After 48 h, cells were collected for further experiments.

Bcl2 overexpression

293T packaging cells were transfected with pCDH-CMV-MCS-EF1-CopGFP-T2A-Puro-Bcl2 or pCDH-CMV-MCS-EF1-CopGFP-T2A-Puro to produce lentiviral particles. The lentivirus was used to transfect C2C12 myotubes. After 24 h, these C2C12 myotubes were used as hosts for transfecting miRNA mimic or NC for 48 h. Myotubes were incubated with anti-MHC. Images were captured by fluorescence microscope (Leica), and the diameter of myotubes was measured by ImageJ.

Immunofluorescent staining

Differentiated C2C12 myotubes were fixed with 4% PFA for 30 min at room temperature, permeabilized with 0.5% Triton X-100 in PBS for 10 min, and then blocked with 5% BSA in PBS for 1 h at room temperature. Myotubes were incubated with anti-MHC (MF-20, 1:100, DSHB) diluted in 5% BSA overnight at 4°C. Myotubes were incubated with secondary antibody Cy3-AffiniPure rabbit anti-mouse IgG (H+L) (1:500, Jackson) at room temperature. Images were captured by fluorescence microscope (Leica), and the diameter of myotubes was measured by ImageJ.

Grip strength

A digital grip-strength meter (YLS-13A, Yiyan Technology, China) was used to measure the grip strength of mice. All mice were acclimatized for 10 min before the grip strength test began. The mice were allowed to grab the metal pull bar. The force was recorded at the time of release as the peak tension. Each mouse was measured six times with a minute break. The experiments were blindly performed by a researcher who did not know the group allocation.

Dual-luciferase assay

When 293T cells were growing in the logarithmic phase, 3.0×10^4 cells were seeded in 24-well plates and cultured at 37°C overnight. 293T cells were co-transfected with the mixture of PGL3-basic-Bcl-2 3′ UTR (wild-type and mutation, removing interaction sequence), *Renilla*, miRNA mimic, and X-tremeGENE 9. Cells were collected after 24 h for dual-luciferase reporter assay. The activation of firefly and *Renilla* luciferase was analyzed with a dual-luciferase reporter assay kit (Promega E1910) according to the manufacturer's guidelines.

TUNEL

The TUNEL Apoptosis Assay Kit (Omega) was used to detect the apoptosis of tissue. For muscle tissue, 4% PFA was used to fix the frozen section. Then, PBS was used to wash the frozen section two times. PBS containing 0.1% Triton X-100 was added to the frozen section. Finally, TUNEL solution (50 μL) was added for staining, and nuclear cells that labeled positively were considered apoptotic cells. The positive cells in six random views were detected with a fluorescence microscope (Leica). The ratio of apoptotic cells was calculated as positive cells/total cells.

Statistical analysis

Data are expressed as mean ± SEM. Two-tailed Student's t test was used for comparisons between two groups. One-way ANOVA test was performed to compare multiple groups, followed by Bonferroni's post hoc test. All analyses were performed with GraphPad Prism 5.0. Values of $p < 0.05$ were considered to be statistically significant and are presented as $^*p < 0.05$, $^{**}p < 0.01$, $^{***}p < 0.001$.

SUPPLEMENTAL INFORMATION

Supplemental information can be found online at https://doi.org/10.1016/j.omtn.2021.04.015.

ACKNOWLEDGMENTS

This work was supported by National Natural Science Foundation of China (no. 81872496, 81873056, and 81772905) and the Science and Technology Commission of Shanghai Municipality (20S11902200 and 16DZ2280100).

AUTHOR CONTRIBUTIONS

X.Z., X.L., and C.M. conceived and designed the study. C.M., W.Z., L.F, X.G., Q.S., S.L., M.F., and Y.L. generated the laboratory data. H.W., X.G., and Y.M. designed and performed the primary clinical study. X.Z., X.L., C.M., and W.Z. interpreted the data. X.Z., X.L., and C.M. wrote the manuscript. All authors critically reviewed the paper and approved of the final version of the paper for submission.

DECLARATION OF INTERESTS

The authors declare no competing interests.

REFERENCES

1. Evans, W.J., Morley, J.E., Argilés, J., Bales, C., Baracos, V., Guttridge, D., Jatoi, A., Kalantar-Zadeh, K., Lochs, H., Mantovani, G., et al. (2008). Cachexia: a new definition. Clin. Nutr. *27*, 793–799.
2. Argilés, J.M., Busquets, S., Stemmler, B., and López-Soriano, F.J. (2014). Cancer cachexia: understanding the molecular basis. Nat. Rev. Cancer *14*, 754–762.
3. Biswas, A.K., and Acharyya, S. (2020). Understanding cachexia in the context of metastatic progression. Nat. Rev. Cancer *20*, 274–284.
4. Busquets, S., Deans, C., Figueras, M., Moore-Carrasco, R., López-Soriano, F.J., Fearon, K.C., and Argilés, J.M. (2007). Apoptosis is present in skeletal muscle of cachectic gastro-intestinal cancer patients. Clin. Nutr. *26*, 614–618.
5. de Castro, G.S., Simoes, E., Lima, J.D.C.C., Ortiz-Silva, M., Festuccia, W.T., Tokeshi, F., Alcântara, P.S., Otoch, J.P., Coletti, D., and Seelaender, M. (2019). Human Cachexia Induces Changes in Mitochondria, Autophagy and Apoptosis in the Skeletal Muscle. Cancers (Basel) *11*, 1264.
6. Baltgalvis, K.A., Berger, F.G., Peña, M.M., Mark Davis, J., White, J.P., and Carson, J.A. (2010). Activity level, apoptosis, and development of cachexia in Apc(Min/+) mice. J. Appl. Physiol. (1985) *109*, 1155–1161.
7. Baracos, V.E., Martin, L., Korc, M., Guttridge, D.C., and Fearon, K.C.H. (2018). Cancer-associated cachexia. Nat. Rev. Dis. Primers *4*, 17105.
8. von Haehling, S., and Anker, S.D. (2014). Prevalence, incidence and clinical impact of cachexia: facts and numbers-update 2014. J. Cachexia Sarcopenia Muscle *5*, 261–263.
9. Argilés, J.M., López-Soriano, F.J., and Busquets, S. (2019). Mediators of cachexia in cancer patients. Nutrition *66*, 11–15.
10. Chitti, S.V., Fonseka, P., and Mathivanan, S. (2018). Emerging role of extracellular vesicles in mediating cancer cachexia. Biochem. Soc. Trans. *46*, 1129–1136.
11. Marinho, R., Alcântara, P.S.M., Ottoch, J.P., and Seelaender, M. (2018). Role of Exosomal MicroRNAs and myomiRs in the Development of Cancer Cachexia-Associated Muscle Wasting. Front. Nutr. *4*, 69.
12. Wu, Q., Sun, S., Li, Z., Yang, Q., Li, B., Zhu, S., Wang, L., Wu, J., Yuan, J., Yang, C., et al. (2018). Tumour-originated exosomal miR-155 triggers cancer-associated cachexia to promote tumour progression. Mol. Cancer *17*, 155.
13. Zhang, H., Zhu, L., Bai, M., Liu, Y., Zhan, Y., Deng, T., Yang, H., Sun, W., Wang, X., Zhu, K., et al. (2019). Exosomal circRNA derived from gastric tumor promotes white adipose browning by targeting the miR-133/PRDM16 pathway. Int. J. Cancer *144*, 2501–2515.
14. Zhang, A., Li, M., Wang, B., Klein, J.D., Price, S.R., and Wang, X.H. (2018). miRNA-23a/27a attenuates muscle atrophy and renal fibrosis through muscle-kidney crosstalk. J. Cachexia Sarcopenia Muscle *9*, 755–770.
15. Conlan, R.S., Pisano, S., Oliveira, M.I., Ferrari, M., and Mendes Pinto, I. (2017). Exosomes as Reconfigurable Therapeutic Systems. Trends Mol. Med. *23*, 636–650.
16. Choi, D.S., Kim, D.K., Kim, Y.K., and Gho, Y.S. (2015). Proteomics of extracellular vesicles: Exosomes and ectosomes. Mass Spectrom. Rev. *34*, 474–490.
17. Hu, W., Ru, Z., Zhou, Y., Xiao, W., Sun, R., Zhang, S., Gao, Y., Li, X., Zhang, X., and Yang, H. (2019). Lung cancer-derived extracellular vesicles induced myotube atrophy and adipocyte lipolysis via the extracellular IL-6-mediated STAT3 pathway. Biochim. Biophys. Acta Mol. Cell Biol. Lipids *1864*, 1091–1102.
18. He, W.A., Calore, F., Londhe, P., Canella, A., Guttridge, D.C., and Croce, C.M. (2014). Microvesicles containing miRNAs promote muscle cell death in cancer cachexia via TLR7. Proc. Natl. Acad. Sci. USA *111*, 4525–4529.
19. Zhang, A., Wang, H., Wang, B., Yuan, Y., Klein, J.D., and Wang, X.H. (2019). Exogenous miR-26a suppresses muscle wasting and renal fibrosis in obstructive kidney disease. FASEB J. *33*, 13590–13601.
20. Wang, B., Zhang, A., Wang, H., Klein, J.D., Tan, L., Wang, Z.M., Du, J., Naqvi, N., Liu, B.C., and Wang, X.H. (2019). *miR-26a* Limits Muscle Wasting and Cardiac Fibrosis through Exosome-Mediated microRNA Transfer in Chronic Kidney Disease. Theranostics *9*, 1864–1877.
21. Miao, C., Lv, Y., Zhang, W., Chai, X., Feng, L., Fang, Y., Liu, X., and Zhang, X. (2017). Pyrrolidine Dithiocarbamate (PDTC) Attenuates Cancer Cachexia by Affecting Muscle Atrophy and Fat Lipolysis. Front. Pharmacol. *8*, 915.
22. Rohm, M., Schäfer, M., Laurent, V., Üstünel, B.E., Niopek, K., Algire, C., Hautzinger, O., Sijmonsma, T.P., Zota, A., Medrikova, D., et al. (2016). An AMP-activated protein kinase-stabilizing peptide ameliorates adipose tissue wasting in cancer cachexia in mice. Nat. Med. *22*, 1120–1130.
23. Tanaka, Y., Eda, H., Tanaka, T., Udagawa, T., Ishikawa, T., Horii, I., Ishitsuka, H., Kataoka, T., and Taguchi, T. (1990). Experimental cancer cachexia induced by transplantable colon 26 adenocarcinoma in mice. Cancer Res. *50*, 2290–2295.
24. Zhou, T., Wang, B., Liu, H., Yang, K., Thapa, S., Zhang, H., Li, L., and Yu, S. (2018). Development and validation of a clinically applicable score to classify cachexia stages in advanced cancer patients. J. Cachexia Sarcopenia Muscle *9*, 306–314.
25. Chen, J., Zhou, R., Liang, Y., Fu, X., Wang, D., and Wang, C. (2019). Blockade of lncRNA-ASLNCS5088-enriched exosome generation in M2 macrophages by GW4869 dampens the effect of M2 macrophages on orchestrating fibroblast activation. FASEB J. *33*, 12200–12212.
26. Catalano, M., and O'Driscoll, L. (2019). Inhibiting extracellular vesicles formation and release: a review of EV inhibitors. J. Extracell. Vesicles *9*, 1703244.
27. Fearon, K., Strasser, F., Anker, S.D., Bosaeus, I., Bruera, E., Fainsinger, R.L., Jatoi, A., Loprinzi, C., MacDonald, N., Mantovani, G., et al. (2011). Definition and classification of cancer cachexia: an international consensus. Lancet Oncol. *12*, 489–495.
28. Kalluri, R., and LeBleu, V.S. (2020). The biology, function, and biomedical applications of exosomes. Science *367*, eaau6977.
29. Daßler-Plenker, J., Küttner, V., and Egeblad, M. (2020). Communication in tiny packages: Exosomes as means of tumor-stroma communication. Biochim. Biophys. Acta Rev. Cancer *1873*, 188340.
30. Huang, W., Yan, Y., Liu, Y., Lin, M., Ma, J., Zhang, W., Dai, J., Li, J., Guo, Q., Chen, H., et al. (2020). Exosomes with low miR-34c-3p expression promote invasion and migration of non-small cell lung cancer by upregulating integrin α2β1. Signal Transduct. Target. Ther. *5*, 39.
31. Zhang, G., Liu, Z., Ding, H., Zhou, Y., Doan, H.A., Sin, K.W.T., Zhu, Z.J., Flores, R., Wen, Y., Gong, X., et al. (2017). Tumor induces muscle wasting in mice through releasing extracellular Hsp70 and Hsp90. Nat. Commun. *8*, 589.
32. Yang, J., Zhang, Z., Zhang, Y., Ni, X., Zhang, G., Cui, X., Liu, M., Xu, C., Zhang, Q., Zhu, H., et al. (2019). ZIP4 Promotes Muscle Wasting and Cachexia in Mice With Orthotopic Pancreatic Tumors by Stimulating RAB27B-Regulated Release of Extracellular Vesicles From Cancer Cells. Gastroenterology *156*, 722–734.e6.
33. Wu, Q., Sun, S., Li, Z., Yang, Q., Li, B., Zhu, S., Wang, L., Wu, J., Yuan, J., Wang, C., et al. (2019). Breast cancer-released exosomes trigger cancer-associated cachexia to promote tumor progression. Adipocyte *8*, 31–45.
34. Yang, D., Zhan, M., Chen, T., Chen, W., Zhang, Y., Xu, S., Yan, J., Huang, Q., and Wang, J. (2017). miR-125b-5p enhances chemotherapy sensitivity to cisplatin by down-regulating Bcl2 in gallbladder cancer. Sci. Rep. *7*, 43109.
35. Chen, Y.Q., Wang, X.X., Yao, X.M., Zhang, D.L., Yang, X.F., Tian, S.F., and Wang, N.S. (2011). MicroRNA-195 promotes apoptosis in mouse podocytes via enhanced caspase activity driven by BCL2 insufficiency. Am. J. Nephrol. *34*, 549–559.
36. Wang, Y., Shao, Y., Gao, Y., Wan, G., Wan, D., Zhu, H., Qiu, Y., and Ye, X. (2018). Catalpol prevents denervated muscular atrophy related to the inhibition of autophagy and reduces BAX/BCL2 ratio via mTOR pathway. Drug Des. Devel. Ther. *13*, 243–253.
37. Zhu, S., Nagashima, M., Khan, M.A., Yasuhara, S., Kaneki, M., and Martyn, J.A. (2013). Lack of caspase-3 attenuates immobilization-induced muscle atrophy and loss of tension generation along with mitigation of apoptosis and inflammation. Muscle Nerve *47*, 711–721.
38. McLoughlin, T.J., Smith, S.M., DeLong, A.D., Wang, H., Unterman, T.G., and Esser, K.A. (2009). FoxO1 induces apoptosis in skeletal myotubes in a DNA-binding-dependent manner. Am. J. Physiol. Cell Physiol. *297*, C548–C555.
39. Nguyen, T.T.N., Choi, H., and Jun, H.S. (2020). Preventive Effects of Dulaglutide on Disuse Muscle Atrophy Through Inhibition of Inflammation and Apoptosis by Induction of Hsp72 Expression. Front. Pharmacol. *11*, 90.

40. Alves, C.R.R., MacDonald, T.L., Nigro, P., Pathak, P., Hirshman, M.F., Goodyear, L.J., and Lessard, S.J. (2019). Reduced sucrose nonfermenting AMPK-related kinase (SNARK) activity aggravates cancer-induced skeletal muscle wasting. Biomed. Pharmacother. *117*, 109197.

41. Yu, Y., Li, X., Liu, L., Chai, J., Haijun, Z., Chu, W., Yin, H., Ma, L., Duan, H., and Xiao, M. (2016). miR-628 Promotes Burn-Induced Skeletal Muscle Atrophy via Targeting IRS1. Int. J. Biol. Sci. *12*, 1213–1224.

42. Yang, X., Xue, P., Chen, H., Yuan, M., Kang, Y., Duscher, D., Machens, H.G., and Chen, Z. (2020). Denervation drives skeletal muscle atrophy and induces mitochondrial dysfunction, mitophagy and apoptosis via miR-142a-5p/MFN1 axis. Theranostics *10*, 1415–1432.

43. Hetzler, K.L., Hardee, J.P., Puppa, M.J., Narsale, A.A., Sato, S., Davis, J.M., and Carson, J.A. (2015). Sex differences in the relationship of IL-6 signaling to cancer cachexia progression. Biochim. Biophys. Acta *1852*, 816–825.